FLOOD MAPPING IN PHRA NAKHON SI AYUTTHAYA, THAILAND, UTILIZING SENTINEL-1 SAR IMAGERY AND DEEP LEARNING APPROACHES

Kritchayan INTARAT [*1,2,3], ***Phatsachon KUANKHAMNUAN*** [1,2], ***Woraman JANGSAWANG*** [1,3]

DOI: 10.21163/GT_2026.211.04

ABSTRACT

This study presents a deep learning (DL)-based flood detection framework for Phra Nakhon Si Ayutthaya Province, Thailand. The framework integrates U-Net architecture with three encoder variants-ResNet50, ResNet101, and ResNet152-using synthetic aperture radar (SAR) imagery from the Sentinel-1 satellite. Model performance is assessed through statistical metrics including accuracy, precision, recall, F1-score, Dice Loss, intersection over union (IoU), and computational time. The U-Net model with a ResNet101 encoder achieved the best performance, with an accuracy of 91.5%, F1-score of 0.886, Dice Loss of 0.116, and IoU of 86.8%, requiring about 24 minutes of training. Despite longer training, the ResNet101-based U-Net substantially enhances flood detection accuracy, highlighting its value as a reliable tool for real-time monitoring and rapid response in flood-prone areas of Thailand.

Key-words: *Flood Detection; SAR Images; U-Net; ResNet; Phra Nakhon Si Ayutthaya Province*

1. INTRODUCTION

Climate variation has expanded the frequency and severity of natural disasters, especially in Southeast Asia. Flooding is a hazard that poses a significant threat to life and property. Among the countries in this region, Thailand experiences flooding almost every year. Particularly prevalent in the lowland terrain, Phra Nakhon Si Ayutthaya Province frequently experiences flooding in many areas. Floods rank among the most destructive natural disasters. Floods consistently generate widespread social and economic challenges across diverse regions, all over the world. Over the past few decades, flood events have become more frequent and more severe (Fakhri & Gkanatsios, 2025; Wang & Feng, 2025).

Climate change, which is resulting in shorter-duration and more intense rainfall, is an influential factor driving this trend. Research indicates that in many parts of the world, the number of areas susceptible to frequent floods is growing (Misra et al., 2025). According to a recent study, water-related disasters made up 48.2% of all disaster events (159 events), more than meteorological disasters (32.1%), climatic disasters (10%, 33 events), and geological disasters (9.7%, 32 events) combined (Sibandze et al., 2025). These figures demonstrate that floods continue to pose a serious threat to the world, especially in light of changing urban land use and environmental conditions. Flooding is also a significant concern in Southeast Asia. Geographical, climatic, and socioeconomic factors all contribute to this vulnerability (Birkmann, 2010; Torti, 2012). Flooding in Thailand has had a profound social and economic impact, destroying many homes and causing extensive property damage.

---

[1]*Research Unit in Geospatial Applications (Capybara Geo Lab), Faculty of Liberal Arts, Thammasat University, Thailand. (KI) intaratt@tu.ac.th, (PK) st125875@ait.ac.th*
[2]*Departement of Geography, Faculty of Liberal Arts, Thammasat University, Thailand.*
[3]*Center of Excellence in Digital Earth Applications and Emerging Technology (CoE: DEET), Sirindhorn International Institute of Technology, Thammasat University, Thailand. (WJ) m6622040878@g.siit.tu.ac.th*

The southwest and northeast monsoons greatly impact Thailand's climate, resulting in periods of high rainfall (Gale et al., 2013). Flooding is made worse by regular and extended rainfall, which is a major contributor to river bank overflows and inundation in the surrounding areas (Loc et al., 2020).

In 2011, many provinces in Thailand were hugely affected. Phra Nakhon Si Ayutthaya Province, in particular, considerably suffered profound social and economic disruption. According to a report by the Dutch Expertise Network for Flood Protection (DENFP), two people were killed and about 6,000 households were impacted by the 400–500 million baht in infrastructure damages (Ghozali et al., 2016). Because of its lowland terrain and the presence of multiple major rivers, Phra Nakhon Si Ayutthaya Province is most vulnerable to flooding that occurs almost annually (Munpa et al., 2022; Hirabayashi et al., 2013). When water levels rise above the river capacity, areas like Phak Hai, Bang Sai, Bang Ban, Sena, and Phra Nakhon Si Ayutthaya districts become flood-retention areas. Planning, managing, and reducing the effects all depend on the detection of floods (Wang et al., 2022). Bentivoglio et al. (2022) reported that traditional assessment techniques suffer from several drawbacks, including limited accuracy across vast regions, high labor demands, and time inefficiency, thereby highlighting the need for more efficient and scalable approaches to flood detection.

In order to overcome the disadvantages of traditional techniques and enhance performance, artificial intelligence (AI) techniques such as machine learning (ML) and deep learning (DL) have been increasingly applied in various fields, such as biomass calculation and carbon sequestration (Angkahad et al., 2024; Angkahad et al., 2025), medical diagnosis (Yang et al., 2021), including water analysis and flood detection (Magyari-Sáska et al., 2025 ; Shoko & Dube, 2024). Disaster risk assessment is one of the many fields that currently use DL techniques (Melgar-García et al., 2023). The processing of spatial data and its application to geographic information is particularly promising for convolutional neural network (CNN) architectures (Intarat et al., 2024).

Regarding the generalization of trained models, DL models still present imperfections. This limitation leads to significant variability when the models are applied across different regions or topographies (Liu et al., 2025). The goal of this work is to improve model performance by applying both U-Net architecture and a CNN designed explicitly for image segmentation to Synthetic Aperture Radar (SAR) data from Sentinel-1 satellites, which are commonly used in hydrological studies (Haidu et al., 2024) and function continuously, both day and night and under all weather conditions (Pech-May et al., 2023; Zhang et al., 2020). This combination will increase the model's capacity to detect flooded areas accurately and generate efficient training data.

This study aims to address these challenges by developing and evaluating a DL-based flood detection framework that integrates the U-Net architecture with multiple encoder variants (ResNet50, ResNet101, and ResNet152) using Sentinel-1 SAR imagery. The models are trained to differentiate between flooded and non-flooded areas at the pixel level by combining VV, VH, and VV–VH composites with a water index for labeling. The efficacy of these encoder configurations is compared using a variety of statistical measures, including precision, recall, F1-score, Dice Loss, and Intersection over Union (IoU), as well as computational efficiency. This strategy not only tackles issues regards computing cost and model generalization, but also enhances flood detection accuracy, providing a solid foundation for operational flood monitoring in complex lowland areas.

2. STUDY AREA

The province of Phra Nakhon Si Ayutthaya is in the middle of Thailand, about 75 kilometers north of Bangkok, covering 2,547.62 square kilometers between 14°6.8450' to 14°40.2925' N and 100°12.7623' to 100°49.3908' E. It borders Ang Thong and Lop Buri to the north, Saraburi to the east, Pathum Thani, Nonthaburi, and Nakhon Pathom to the south, and Suphan Buri to the west (**Fig. 1**). The province's land is mostly lowland terrain (2 to 20 meters elevation) intersected by three major rivers (Chao Phraya, Pa Sak, Lopburi) and numerous canals that support irrigation, transportation, and flood drainage. The average temperature in Phra Nakhon Si Ayutthaya is about 28.4 °C all year round, summer peaks above 40 °C, and annual rainfall of 1,000–2,000 mm, with most of it falling between May and October, resulting in a tropical savanna climate.

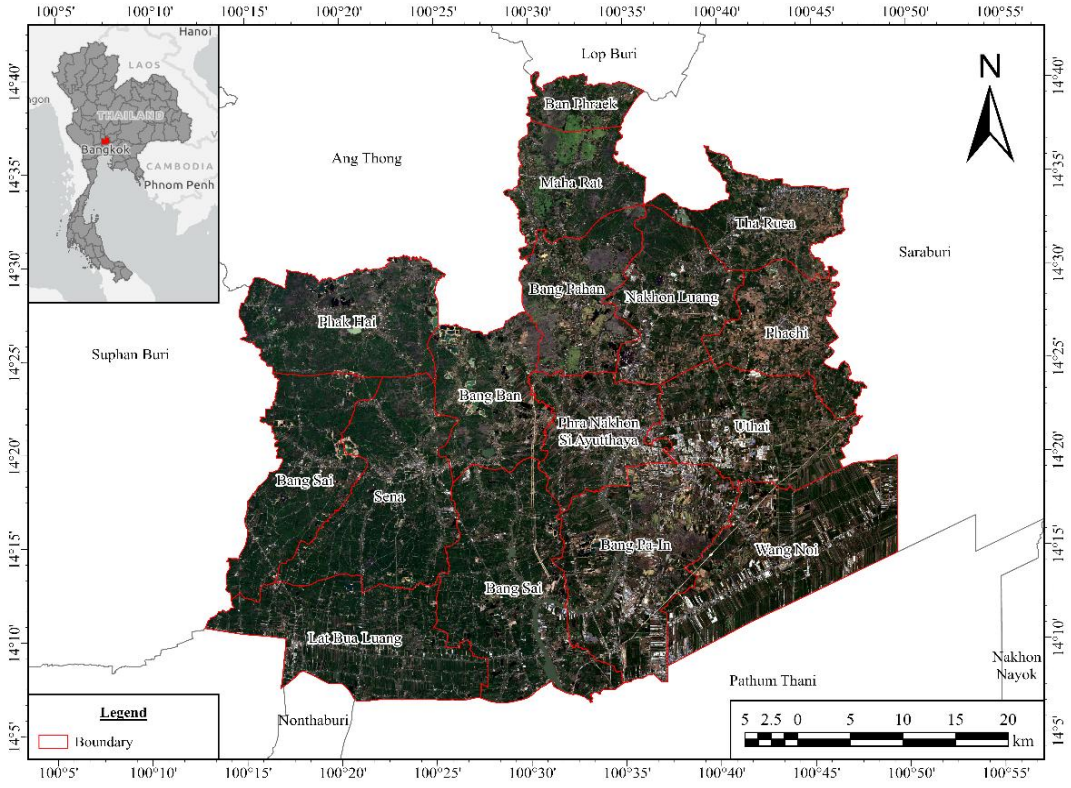

Fig. 1. The study area: Phra Nakhon Si Ayutthaya Province, Thailand.

The province is one of Thailand's leading agricultural and industrial hubs, with numerous rice paddies and several large industrial estates that contribute significantly to the country's manufacturing output. It is also of cultural and historical importance as the site of the ancient Ayutthaya Kingdom, a UNESCO World Heritage Site. However, its extensive lowlands, dense river network, and rapid urban-industrial growth make the area highly prone to severe flooding during the monsoon season, providing a critical case study for flood detection and risk management in Thailand's central plains.

3. DATA AND METHODS

3.1. Remote sensing (RS) data

This study selected Sentinel-1 SAR data operated by the European Space Agency (ESA) in ground range detected (GRD) format on September 28, 2024, derived from the Google Earth Engine platform. The imagery was already pre-processed through four main steps: thermal noise removal, radiometric calibration, terrain corrections, and speckle filtering (Ponmani & Saravanan, 2021). This imagery includes both VV and VH polarization. To give the model more information, VV, VH, and VV-VH polarization overlays were added. Then, we calculated the water index (WI) as a criterion for thresholding in our study area (Wu et al., 2023). The threshold is set between 0.2 and 2. It enables us to distinguish between flooded and non-flooded areas in SAR imagery during flood events. WI can be expressed as in Eq. (1):

$$WI = \ln(10 \times VH \times VV) - 8 \quad (1)$$

where WI represents water index, VH and VV refer to Sentinel-1 SAR polarizations.

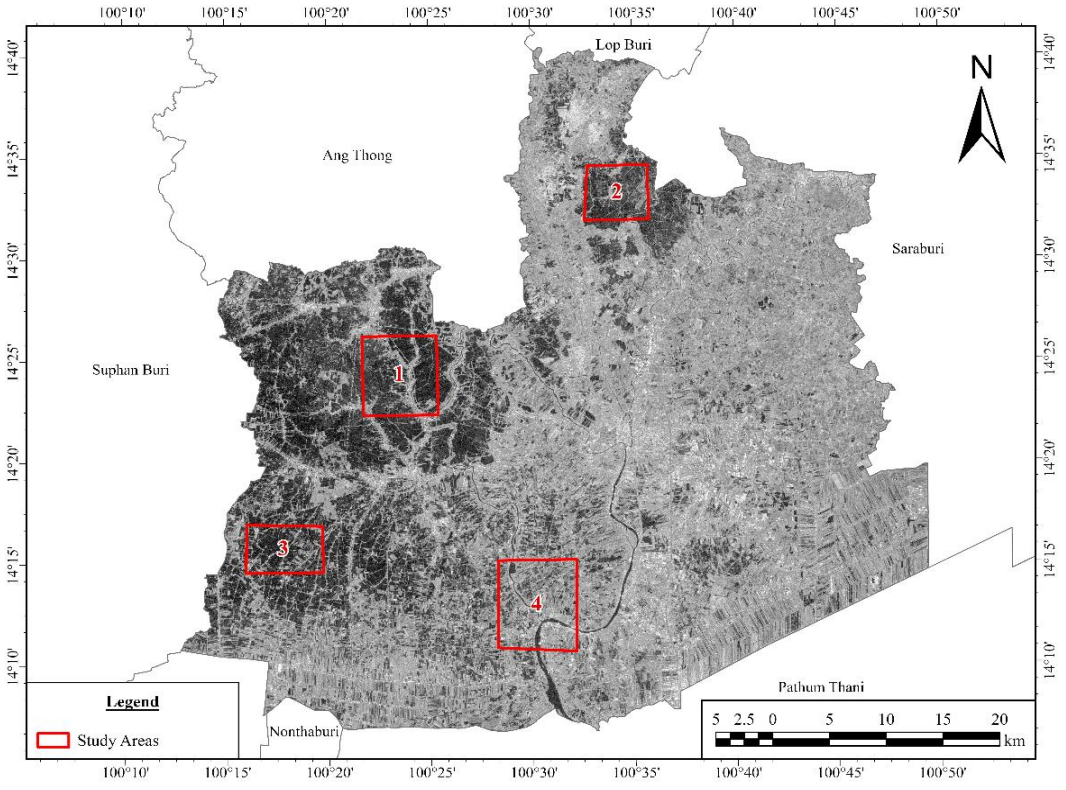

Fig. 2. Sentinel-1 SAR imagery showing four acquired samples used for model training (red bounding boxes).

The aforementioned method facilitated a preliminary distinction between flooded and non-flooded areas, which was subsequently used to assist in generating labels for the dataset. To enhance accuracy and reduce the time required for computation, four representative sites within Phra Nakhon Si Ayutthaya Province were delineated (**Fig.2**). The results obtained from WI calculations along with SAR imagery with overlaid with VV, VH, VV-VH polarizations were employed to construct dataset for model training and testing. The sample areas encompassed diverse land cover types, including flood-prone zones and riverine areas. In addition, the samples were spatially distributed to improve the model's robustness and accuracy (Wu et al., 2023).

All experiments were conducted on a high-performance workstation equipped with an Intel Xeon E5-2696V2 2.5 GHz processor, 128 GB of RAM, and an NVIDIA GeForce GTX 1080 Ti GPU with 11 GB of VRAM. The system ran Ubuntu 24.04 LTS, which is compatible with deep learning workflows and provides a stable and optimized environment. This setup enabled the quick processing of large Sentinel-1 SAR datasets, reducing the time required to train the models.

3.2. U-Net model

CNNs are the foundation of the deep learning architecture known as U-Net (Ronneberger et al., 2015). It is intended for pixel-level image segmentation (Konovalenko et al., 2022; Liu et al., 2020), especially for applications that call for accurate spatial delineation. The two primary components of U-Net's structure are the encoder (contracting path), which uses convolution, ReLU activation, and Max Pooling to extract deep image features and reduce the image's dimensionality, plus the decoder (expanding path), which upscales the image using transposed convolution and uses skip connections to connect the data to the original encoder layer (Melgar-García et al., 2023).

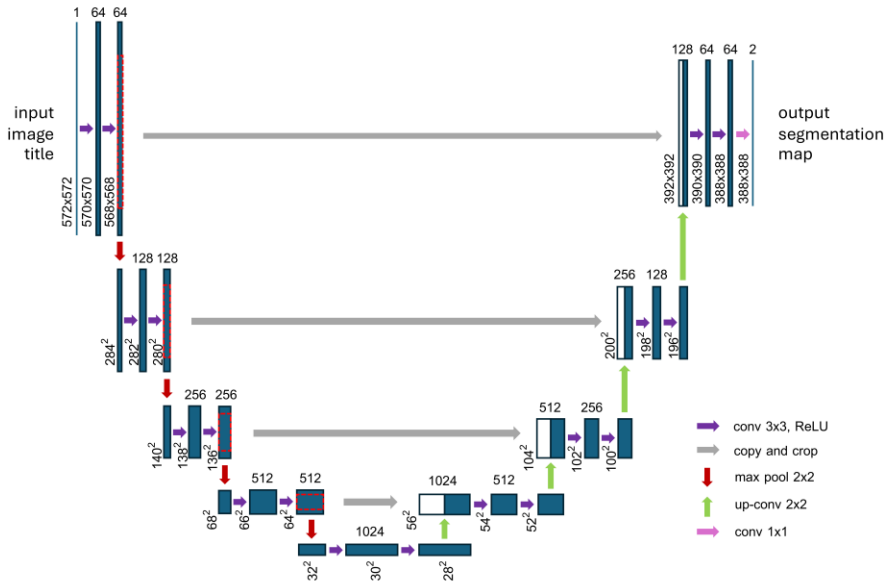

Fig. 3. The structure of U-Net: encoder-decoder with skip connections for image segmentation.

In **Fig. 3**, the U-Net's architecture is illustrated. In such an architecture, meaningful spatial information is preserved. It also improves the effectiveness of segmentation. According to Zhou et al. (2018), the outcome offers a very detailed segmented imagery that enables the U-Net to identify complex regions precisely.

U-Net has the advantage of being able to preserve spatial details and function effectively with a small dataset. It can also be applied to both optical and SAR imagery, including Sentinel-1 and Sentinel-2 (Konapala et al., 2021; Muszynski et al., 2022; Zhao et al., 2022). In addition, U-Net has demonstrated exceptional efficacy in flood mapping, particularly when applied to SAR imagery, which is weather-independent and capable of acquiring data both day and night. For instance, Ghosh et al. (2024) used Sentinel-1 SAR data to create a U-Net model for flood mapping. They discovered that it could precisely detect flooded areas even when there was cloud cover. Similarly, in order to map floods from high-resolution satellite data for prompt disaster response, Bonafilia et al. (2020) created a flood mapping model (FMM) based on U-Net architecture. When Dhanabalan et al. (2021) combined Sentinel-1 and Sentinel-2 data with a U-Net, they were able to monitor flooded areas in Kerala, India, with greater accuracy than conventional methods. According to its capabilities, U-Net can effectively apply Sentinel data, preserve spatial data in regions with complex terrain, and precisely determine flood extents.

3.3. ResNet encoder

The vanishing gradient and network degradation issues that are frequently present in deep models can be resolved by the DL architecture ResNet (He et al., 2016). The Residual Block, which consists of learning sub-functions and shortcut connections or identity mapping that enable the input to be passed straight to the next layer, is the primary mechanism of this architecture (Liu et al., 2023). The output is then obtained by adding the results of the sub-functions. This method enhances the training stability of networks with hundreds of layers. It makes deep model training more effective (He et al., 2016; Zhong et al., 2017).

ResNet architecture has been designed in multiple versions, including ResNet50, ResNet101, and ResNet152 (Intarat et al., 2024). The capabilities of ResNet include its fast convergence, complex hierarchical feature learning, adaptability to further development into better architectures like

ResNeXt or Attention-ResNet, and its ability to be applied to very deep networks without gradient loss (Yang et al., 2022; Hassan & Maji, 2024; Intarat et al., 2024). Some drawbacks include high computational resource demands, the risk of overfitting with limited training data, and the need for structural adjustments when handling temporal data. Due to its proven ability, ResNet was incorporated into our U-Net model to learn complex deep features, adapt to varying resource constraints when determining model depth, and perform well across diverse image processing tasks. These advantages make ResNet a strong choice for tasks requiring both effective hierarchical deep learning and spatial precision.

3.4. Hyperparameter tuning

Tuning hyperparameters is an important step that can significantly improve the performance of the DL model. These hyperparameters define the model's architecture and learning process parameters (Mukherjee et al., 2024). In **Table 1**, the initial hyperparameters used in our study are shown. Correctly defining the retirees' demarcation may help the model learn more effectively from limited input data. It can also reduce the risk of overfitting or underfitting and improve the model's generalization when applied to other datasets.

Table 1.

Hyperparameters of the U-Net model used in this study.

Hyperparameter	Detail
Input shape	128 × 128 pixel
Batch size	32
Optimizer	Adam
Loss function	Dice loss
Activation function	Sigmoid
Epoch	500
Encoder	ResNet50, ResNet101, and ResNet152
Encoder weight	ImageNet

According to **Table 1**, initial hyperparameters were set to train three models using different encoder architectures e.g. ResNet50, ResNet101, and ResNet152; hyperparameter tuning results in spatial details preservation and significant accuracy improvement. Lee et al. (2022) suggested that tuning the patch size, kernel size, and model structure provides higher precision and reduces validation loss significantly. Das et al. (2022) found that considering an appropriate optimizer and loss function can accelerate convergence and increase segmentation efficiency. Systematic hyperparameter fine-tuning not only helps increase the model's precision but also provides reliability and repeatability.

3.5. Model training and testing

According to information obtained in the previous step, the dataset was created by slicing the images into 128 x 128 pixels tiles. Then, these tiles were split into two sets: 80% for training and 20% for testing (Sazara et al., 2019). After the training, the model was used to predict and discriminate between flooded and non-flooded areas across the entire area. To evaluate the model' s performance, the confusion matrix was associated with and delivered accuracy (Eq. (2)), precision (Eq. (3)), recall (Eq. (4)), and F1-score (Eq. (5)) (Amitrano et al., 2024). Each metric was calculated using true positive (TP), true negative (TN), false positive (FP), and false negative (FP) and expressed, accordingly:

$$Accuracy = \frac{TP+TN}{TP+TN+FP+FN} \quad (2)$$

$$Precision = \frac{TP}{TP+FP} \quad (3)$$

$$Recall = \frac{TP}{TP+FN} \quad (4)$$

$$F1 - score = \frac{2\ x\ Precision\ x\ Recall}{Precision+Recall} \quad (5)$$

The model' s performance was also evaluated using the Dice Loss method (Pech-May et al., 2024), as it reflects accurate image segmentation, by comparing the overlap between predicted results and the ground truth. We also applied the IoU method (Eq. (6)) in the four sample areas mentioned earlier to examine the overlap between the predicted area and the actual ones (Safarov et al., 2022).

$$IoU = \frac{|A \cap B|}{|A \cup B|} \quad (6)$$

where A refers to the predicted flood area and B reveals the actual flood area.

IoU lies between 0 and 1 (0 - 100%): a value close to 1 indicates high predictability of the model. IoU can also estimate positional accuracy and completeness in flood segmentation (Mosinska et al., 2018; Jamali et al., 2024). The comparison also included the evaluation of training time.

4. RESULTS

4.1. Model evaluation and comparison

Herein, we thoroughly tested the performance of the U-Net models that used ResNet50, ResNet101, and ResNet152 encoders using a variety of performance metrics, such as accuracy, precision, recall, F-1 score, and Dice Loss. **Table 2** presents a detailed summary of how well the model worked.

Table 2.

Evaluation Results of U-Net Models with ResNet50, ResNet101, and ResNet152 encoders.

Metric	ResNet50	ResNet101	ResNet152
Accuracy	0.9164	0.9154	0.9100
Precision	0.8790	0.8617	0.8476
Recall	0.8736	0.9118	0.9148
F1-score	0.8858	0.8860	0.8799
Dice Loss	0.1149	0.1161	0.1233

As shown in **Table 2**, the ResNet50 encoder achieved the highest overall accuracy (0.9164), surpassing ResNet101 (0.9154) and ResNet152 (0.9100). It also exhibited the highest precision (0.8790), indicating superior ability to identify flooded areas while minimizing misclassification of non-flooded pixels. ResNet101 and ResNet152 followed with precision scores of 0.8617 and 0.8476, respectively. In contrast, the recall scores displayed a different pattern: ResNet152 achieved the highest recall (0.9148), followed by ResNet101 (0.9118), with ResNet50 slightly lower at 0.8736.

The F-1 scores, which balance precision and recall, proved to be similar across models. The ResNet50 and ResNet101 encoders achieved almost identical scores (0.8858 and 0.8860, respectively), whereas the ResNet152 model scored slightly lower (0.8799). The ResNet50 model had the lowest Dice Loss value (0.1149), followed by ResNet101 (0.1161) and ResNet152 (0.1233). Dice Loss is inversely related to segmentation accuracy, so lower values mean better performance. As such, it supports the idea that the ResNet50 encoder provides the best overall segmentation performance. In **Fig.4**, the evaluation of ResNet encoder performance is presented. In **Figs. 5-9**, all statistical metrics are exhibited.

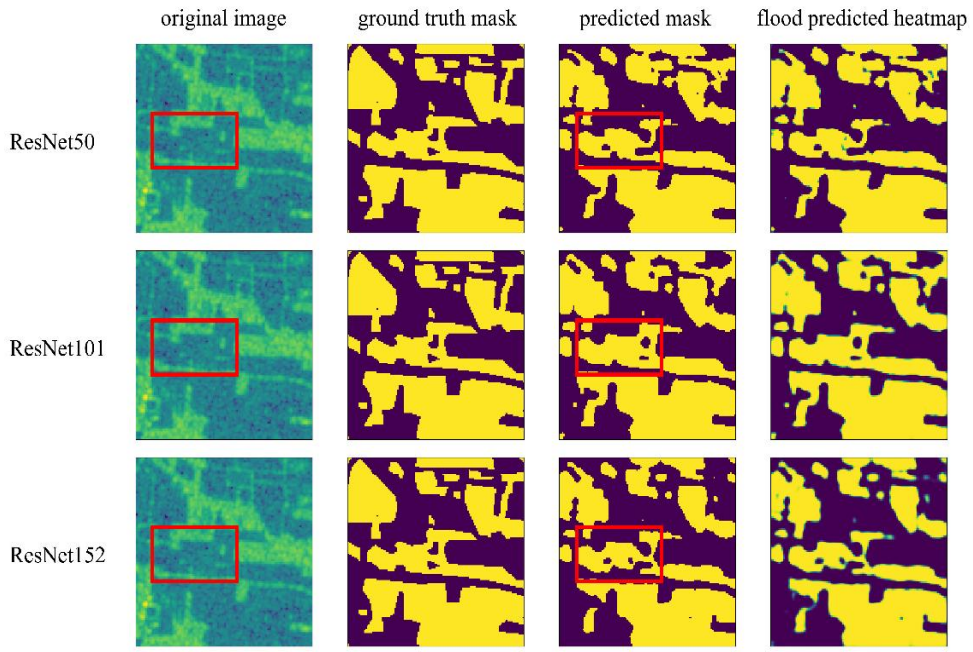

Fig. 4. Examples of U-Net model predictions using ResNet50, ResNet101, and ResNet152 encoders, showing that ResNet101 provides the most accurate predictions.

In **Fig. 4**, the U-Net model is illustrated detecting floods in Sentinel-1 SAR imagery using three encoder configurations: ResNet50, ResNet101, and ResNet152. Each panel displays the predicted flooded and non-flooded areas overlaid on the study area, making it straightforward to witness how well the segmentation works at different encoder depths. Results demonstrate that the ResNet101 encoder produces the most accurate and spatially consistent predictions. It draws flood boundaries with greater precision and fewer blunders than the ResNet50 and ResNet152 configurations. The visual observations correspond to the testing values in Table 2, which reveal that the ResNet101-based model had the best balance between recall and F1-score, supporting its overall superior performance. **Figs. 5-9** illustrate the training performance of U-Net models with ResNet50, ResNet101, and ResNet152 encoders. Overall, the curves show how the models converged and balanced segmentation trade-offs. In **Fig. 5**, all three models improved at making accurate predictions over time, with variability decreasing significantly after the first few iterations. ResNet101 encoder had the most stable and consistent accuracy trajectory. In **Fig. 6,** the precision curves exhibit greater variation than the accuracy curves, particularly during the early epochs to improved at making accurate predictions, while ResNet101 encoder exhibited the most consistent precision.

In contrast, **Fig. 7**, the recall curve was more stable for ResNet50, suggesting reliable detection of flooded areas, though with a higher false-positive rate, resulted in a lower overall recall compared to ResNet101 and ResNet152. **Fig. 8** presents the F1-score curves, which reflect the balance between precision and recall, even ResNet50 showed the lowest variance, ResNet101 achieved the highest overall F1-score. Finally, **Fig.9** presents the Dice Loss curves, with the ResNet50 encoder exhibiting the lowest and most stable values, indicating its ability to consistently delineate boundaries.

In **Table 3**, IoU performance for the four sample areas is presented. The ResNet101-based U-Net model achieved the highest average IoU (86.84%). It also achieved the highest IoU in samples 1, 3, and 4 (94.86%, 94.61%, and 65.26%, respectively). Although ResNet152 attained the best IoU in sample 2 (94.53%), ResNet101 demonstrated the highest and most consistent overall IoU performance.

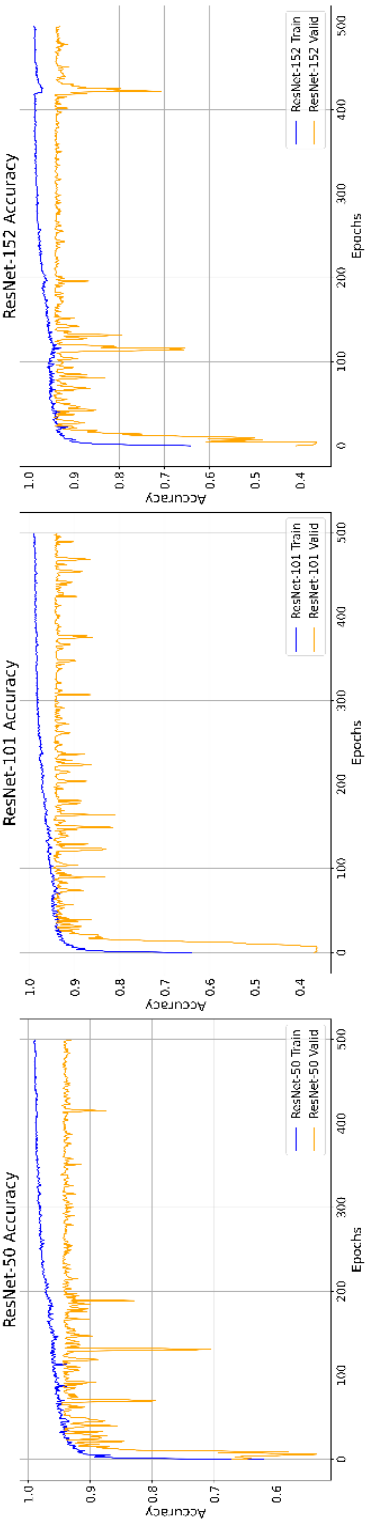

Fig. 5. Training and validation Accuracy of the U-Net model with ResNet50, ResNet101, and ResNet152 encoders. Accuracy values indicate the proportion of correctly predicted areas, both flooded and non-flooded, ResNet101 exhibited the most stable and consistent accuracy compared to ResNet50 and ResNet152.

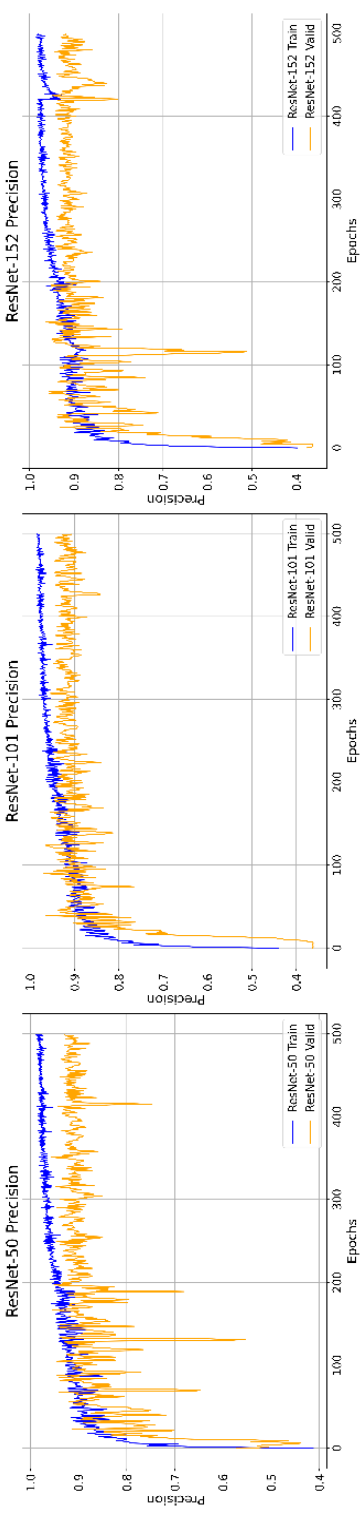

Fig. 6. Training and validation Precision of the U-Net model with ResNet50, ResNet101, and ResNet152 encoders. Precision values indicate the proportion of correctly predicted flooded areas among all areas predicted as flooded. ResNet101 shows more stable and consistent Precision compared to ResNet50 and ResNet152.

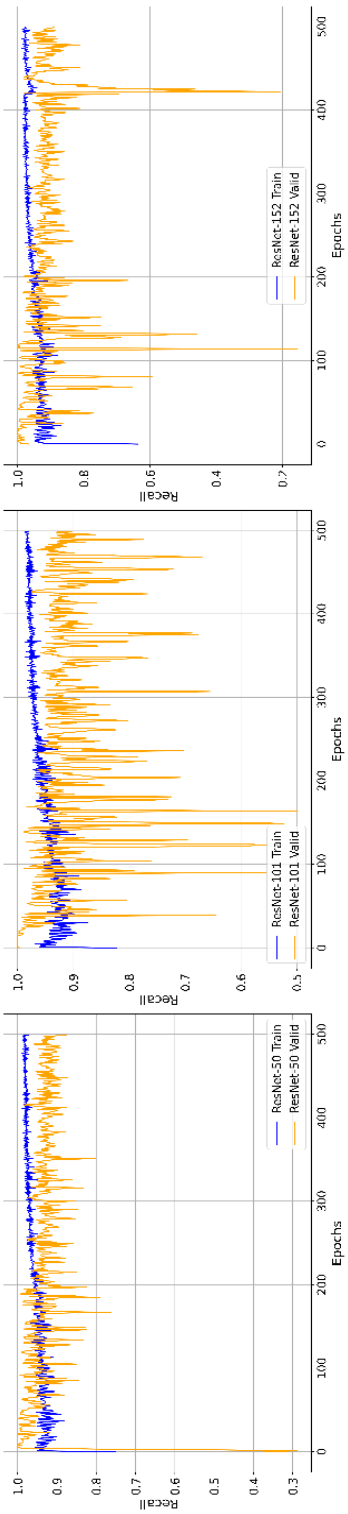

Fig. 7. Training and validation Recall of the U-Net model with ResNet50, ResNet101, and ResNet152 encoders. Recall values indicate the model's ability to correctly identify flooded areas. While ResNet50 demonstrated more stable Recall, ResNet101 and ResNet152 encoders achieved higher overall Recall values.

Fig. 8. Training and validation F1-score of the U-Net model with ResNet50, ResNet101, and ResNet152 encoders. F1-score indicates the balance between Precision and Recall. ResNet50 and ResNet101 achieved more stable and consistent performance compared to ResNet152.

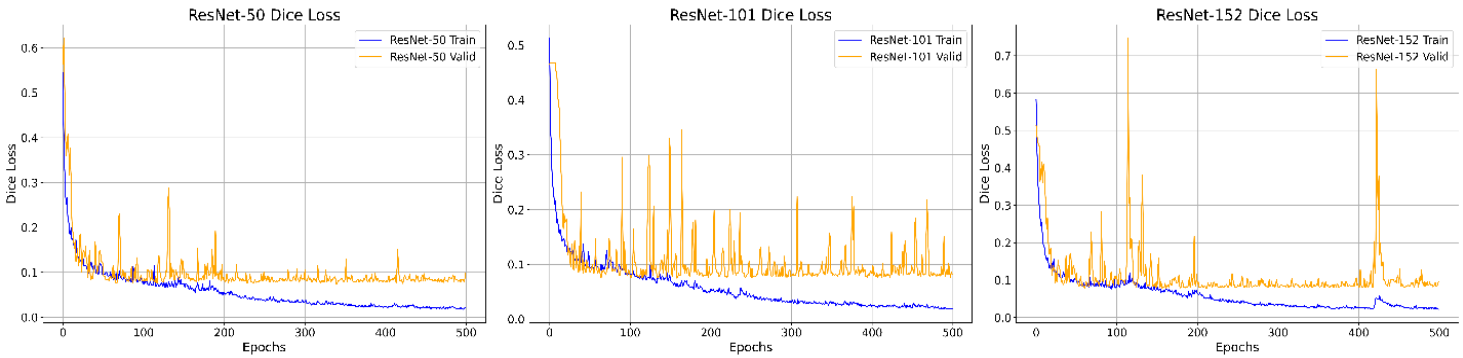

Fig. 9. Training and validation Dice Loss of the U-Net model with ResNet50, ResNet101, and ResNet152 encoders. Lower Dice Loss values indicate higher segmentation performance. ResNet50 and ResNet101 encoders showed more stable convergence, while ResNet152 exhibited greater loss variance.

Table 3.
IoU results for the four sample areas, showing the overlap between predicted and actual flood extents.

Sample	ResNet50	ResNet101	ResNet152
1	94.1431	94.8647	93.6507
2	92.7707	92.6230	94.5297
3	92.5100	94.6137	92.0071
4	59.5352	65.2567	53.8099
average (mean)	84.7398	86.8395	83.4994

Table 4.
U-Net model computational time using different ResNet encoders.

Encoder	Runtime
ResNet50	22 min 14 sec
ResNet101	24 min 04 sec
ResNet152	32 min 00 sec

Table 4 reports the time comsumption of each model training. The computational overhead of ResNet152 (32 min) was considerably higher than that of ResNet50 (22 min 14 sec) and ResNet101 (24 min 4 sec). This underscores the operational cost of employing excessively deep encoders in near-real-time applications.

4.2. Map of flooded areas in Phra Nakhon Si Ayutthaya Province

The U-Net model with the ResNet101 encoder generated flood maps for Phra Nakhon Si Ayutthaya Province on October 28, 2024. In our evaluation, it offered the best overall balance between precision, recall, and IoU. In **Fig.10**, the spatial distribution of the detected inundation is shown. Extensive flooding was observed in the eastern and northern regions of the province—specifically, the districts of Phak Hai, Bang Sai, Bang Ban, and Sena. These areas correspond to agricultural zones and low-lying floodplain regions, which act as natural retention basins when water levels rise above the capacity of the riverbanks.

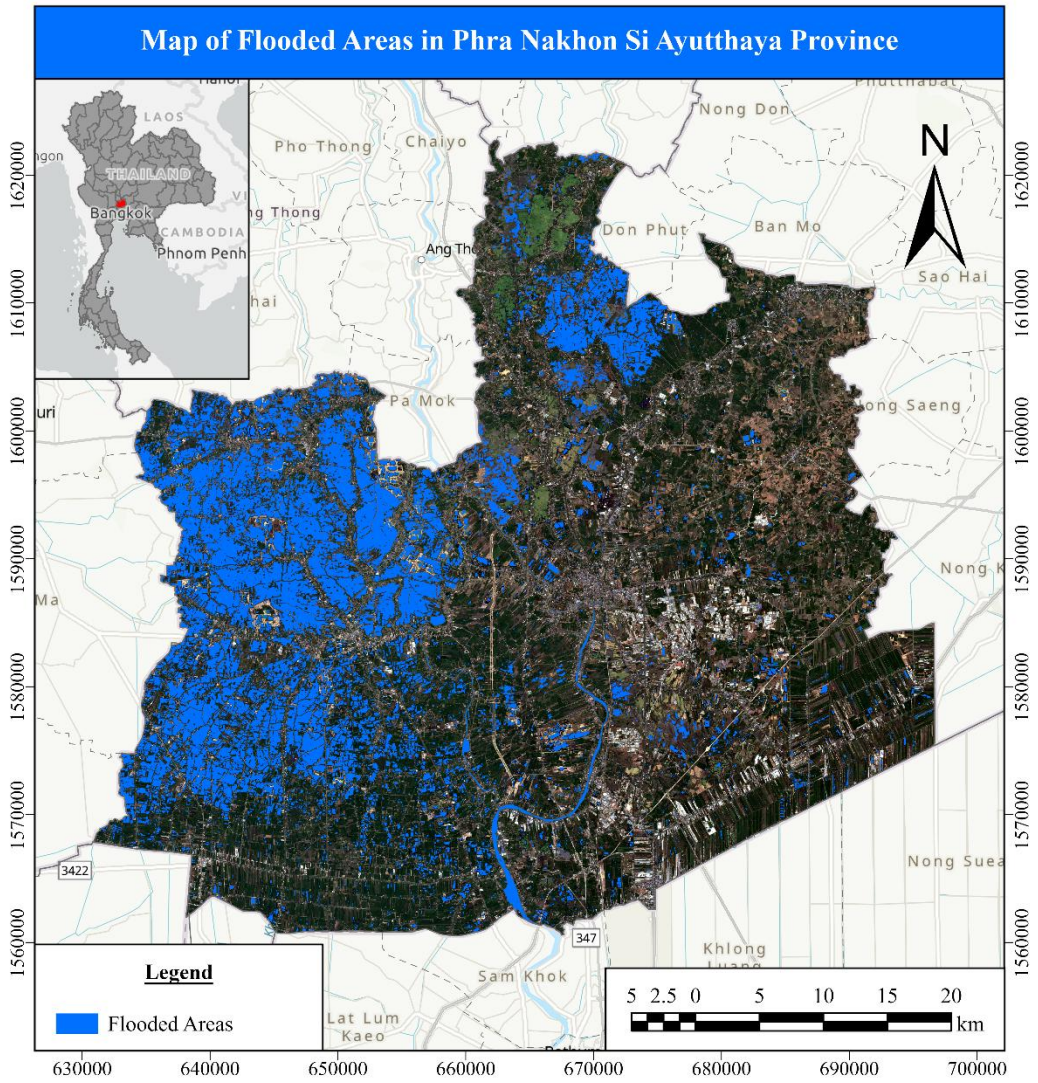

Fig. 10. Flood detection map in the study area on October 28, 2024. The blue areas represent regions identified as flooded based on U-Net model with ResNet101 encoder.

5. DISCUSSIONS

The flood detection model for Phra Nakhon Si Ayutthaya Province was constructed by integrating the ResNet architecture into U-Net, trained by SAR imagery classified into flooded and non-flooded areas. SAR data offers detailed spatial information and is unaffected by cloud cover, making it particularly suitable for flood mapping. Reducing the model's runtime by selecting only four study areas from the entire province contributed to improving detection efficiency. Overall, the U-Net model with ResNet101 encoder demonstrated the highest performance. The model performed well across all evaluation metrics, particularly with significantly higher recall and F1-score than ResNet50 and ResNet152, compared to other evaluation metrics. Additionally, the U-Net model with ResNet101 encoder achieved the highest average IoU and required only 2 min more runtime than ResNet50. The results from experiments with different ResNet encoders indicate that, although the ResNet50-based model benefits from the shortest runtime, its relatively shallow architecture may limit its ability to fully capture the data in certain cases. On the other hand, ResNet152, the deepest network of the three networks, may make the model unnecessarily complex and encounter overfitting problems as well as requiring the longest runtime, which can be a problem when dealing with large datasets or time-sensitive tasks. These results suggest that deeper encoders, such as ResNet101 and ResNet152, may be more effective at capturing flooded areas comprehensively, but this advantage can come at the cost of lower accuracy, resulting in more false positives.

However, the U-Net model with the ResNet101 encoder may not always outperform ResNet50 or ResNet152, particularly when hyperparameter tuning—such as increasing the number of training epochs—is considered. Such tuning often entails higher computational cost and longer processing time. Therefore, the availability of computational resources, model efficiency, and runtime requirements should be considered when selecting an appropriate model. In this study, the model did not achieve perfect accuracy in flood detection (**Fig. 11**). To further enhance performance, future research could investigate advanced deep learning approaches, such as multi-scale DeepLab (Wu et al., 2022).

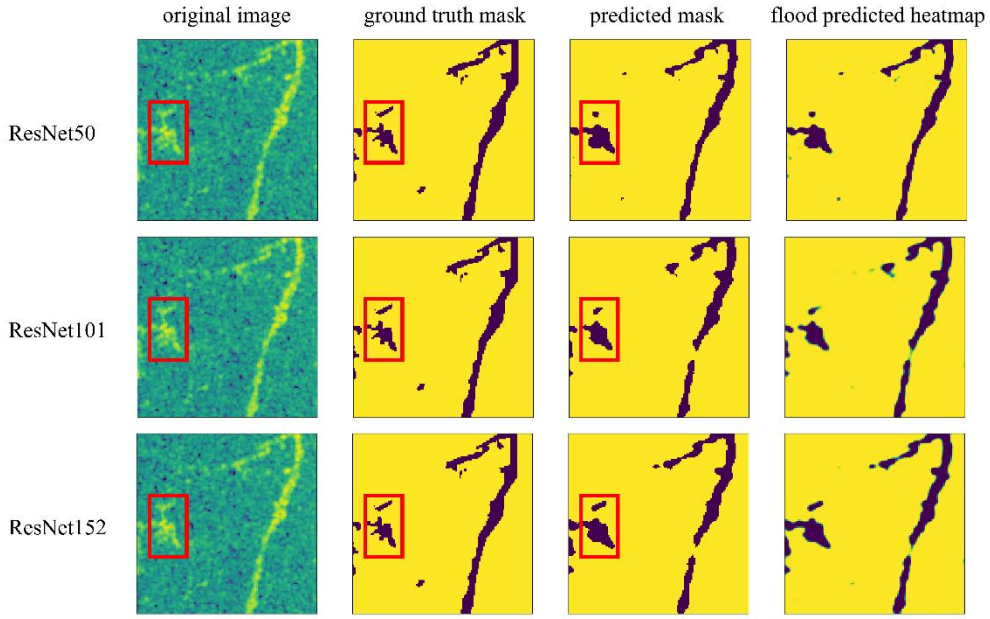

Fig. 11. Example of imperfect predictions using U-Net model with ResNet50, ResNet101, and ResNet152 encoders.

Additionally, using training data with higher resolution and accuracy could contribute to better model generalization (Ardohain & Fei, 2025). Incorporating multi-event and multi-temporal datasets can also enhance model performance (Magyari-Sáska et al., 2025) by capturing flood dynamics under diverse hydrological and environmental conditions. Such data could reduce event-specific bias and enhance the model's transferability to unseen flood scenarios or areas with different hydrological or topographic characteristics. (Wu et al., 2023). Future work should be integrated with temporal analysis, such as comparing SAR images from pre-flood and flood periods, to detect changes in surface water extent and identify only flooded areas (Yadav et al., 2022).

Moreover, the findings of the present study indicate that ResNet-101 often provides an optimal balance between network depth and generalization performance in image classification tasks. Similar patterns have been observed in previous studies (Pan et al., 2023; Shokati et al., 2025; Ait EI Asri et al., 2023) which found that ResNet101 achieved superior performance and often struck a good balance between feature extraction and the prevention of overfitting (He et al., 2016; Liu et al., 2020). compared with ResNet50 and ResNet152, despite not being the deepest architecture. These results highlight that a more complex model does not guarantee better performance (Pan et al., 2023) and may not work as well for segmentation tasks with SAR data (Pech-May et al., 2023). Although ResNet50 demonstrated the lowest training loss among the tested architectures, its performance on the validation set was markedly lower than that of ResNet101. This outcome suggests that ResNet50 being relatively compact and shallow was prone to overfitting and incapable of capturing complex and subtle patterns (Pan et al., 2023; Li et al.,2022). Taken together, these findings provide further evidence that ResNet101 offers a robust and efficient architecture for image-based detection tasks. During prediction testing, model performance was evaluated using IoU. ResNet101 achieved outstanding performance, with an IoU of 86.84%, demonstrating superior predictive capability. Such a model provided the best results for the samples within area boundaries one, three, and four (see the red boundaries in **Fig.2**). In contrast, the sample in boundary two is aligned with the ResNet50 encoder.

However, based on model evaluation, the ResNet152 encoder achieved the highest recall (0.9148) but underperformed in precision (0.8476) and overall IoU. This issue reflected a tendency to over-segment flooded areas and introduce false positives. This finding aligns with previous studies, which emphasize that very deep encoders can increase model complexity and training time without proportionally improving segmentation quality (Bonafilia et al., 2020; Liu et al., 2020). ResNet152 also required the longest computational time compared to the other encoders (**Table 4**), highlighting the trade-off between encoder depth and computational efficiency. Deeper networks introduce additional overhead without necessarily improving segmentation performance.

This study demonstrates that our flood detection model is capable of accurately delineating flood extents. The generated flood maps can be integrated into existing disaster management frameworks in Thailand, such as Thailand Incident Command System of the Department of Disaster Prevention and Mitigation (DDPM). Such integration has the potential to support spatial decision-making and strengthen operational response during flood events. To enable the developed model to be effectively deployed in real-world scenarios, improvements in computational infrastructure, processing, and data storage capabilities are required. The effectual model includes the use of higher-performance servers or workstations, particularly for larger datasets, especially when extending analyses to a national scale. Furthermore, addressing computational latency is crucial to ensure timely decision-making during flood events. To address the limitations arising from computational time, adopting models with lower architecture complexity yet comparable performance, such as ResNet50, may provide a practical solution. This approach would help reduce computational latency and resource demand, thereby improving the feasibility of real-time deployment.

By systematically comparing three encoder depths, we demonstrated that the ResNet101-based U-Net represents the best choice for mapping floods in complex lowland areas such as Phra Nakhon Si Ayutthaya Province. These results address a key research gap by providing a robust and generalizable deep learning model capable of balancing accuracy, stability, and computational efficiency in flood detection. This study provides novel insights into optimizing U-Net architectures

for flood mapping using SAR imagery through the evaluation of different encoder depths. The results are applicable to large-scale flood monitoring and the strategic planning of emergency response operations.

6. CONCLUSIONS

This study developed a U-Net-based flood detection framework for Phra Nakhon Si Ayutthaya Province, using Sentinel-1 SAR imagery combined with ResNet-50, ResNet-101, and ResNet-152 encoders. Results demonstrated that the ResNet-101 encoder offered the best balance between segmentation performance and computational efficiency, making it the optimal choice for operational flood mapping.

The flood maps constructed for the October 2024 event aligned with past flood patterns and successfully identified the province's most at-risk areas, underscoring the model's reliability for hazard assessment.

From a practical perspective, the proposed framework is scalable and provides an effective means for near real-time flood monitoring, thereby aiding disaster management. Future research should explore multi-temporal SAR data, integration with optical and LiDAR sources, and advanced architectures to further enhance generalization and boundary detection in complex environments.

ACKNOWLEDGEMENT

This research was supported by the Faculty of Liberal Arts, Thammasat University, Research Unit în Geospatial Applications (Capybara Geo Lab). It is aslo partailly supported by the Center of Excellence in Digital Earth and Emerging Technology (CoE: DEET), Thammasat University, Pathumthani, Thailand, 12120.

REFERENCES

Ait El Asri, S., Negabi, I., El Adib, S., & Raissouni, N. (2023). Enhancing building extraction from remote sensing images through UNet and transfer learning. *International Journal of Computers and Applications*, *45*(5), 413-419. https://doi.org/10.1080/1206212X.2023.2219117

Amitrano, D., Di Martino, G., Di Simone, A., & Imperatore, P. (2024). Flood Detection with SAR: A Review of Techniques and Datasets. *Remote Sensing*, 16(4), 656. https://doi.org/10.3390/rs16040656

Angkahad, T., Laosuwan, T., Sangpradid, S., Prasertsri, N., Uttaruk, Y., Phoophathong, T., & Nuchthapho, J. (2024). An Empirical Analysis of Above Ground Biomass and Carbon Sequestration Utilizing UAV Photogrammetry and Machine Learning Techniques. *IEEE Access*, 12, 186740-186752. https://doi.org/ 10.1109/ ACCESS.2024.3514074

Angkahad, T., Laosuwan, T., Sangpradid, S., Prasertsri, N., Uttaruk, Y., Phoophathong, T., & Nuchthapho, J. (2025). Developing a Drone-Based Machine Learning for Spatial Modeling and Analysis of Biomass and Carbon Sequestration in Forest Ecosystems. *Engineered Science*, 35, 1508. http://dx.doi.org/10.30919 /es1508

Ardohain, C., & Fei, S. (2025). The impacts of training data spatial resolution on deep learning in remote sensing. *Science of Remote Sensing*, 11, 100185. https://doi.org/10.1016/j.srs.2024.100185

Bentivoglio, R., Isufi, E., Jonkman, S. N., & Taormina, R. (2022). Deep learning methods for flood mapping: a review of existing applications and future research directions. *Hydrology and Earth System Sciences Discussions*, 26(16), 1-50. https://doi.org/10.5194/hess-26-4345-2022

Birkmann, J., Buckle, P., Jaeger, J., Pelling, M., Setiadi, N., Garschagen, M., Fernando, N., & Kropp, J. (2010). Extreme events and disasters: a window of opportunity for change? Analysis of organizational, institutional and political changes, formal and informal responses after mega-disasters. *Natural Hazards*, 55, 637-655. https://doi.org/10.1007/s11069-008-9319-2

Bonafilia, D., Tellman, B., Anderson, T., & Issenberg, E. (2020). Sen1Floods11: A georeferenced dataset to train and test deep learning flood algorithms for sentinel-1. *Proceedings of the IEEE/CVF conference on computer vision and pattern recognition workshops*, pp. 210-211. https://doi.org/10.1109/CVPRW50498.2020.00113

Das, S., Swain, M. K., Nayak, G. K., Saxena, S., & Satpathy, S. C. (2022). Effect of learning parameters on the performance of U-Net Model in segmentation of Brain tumor. *Multimedia tools and applications*, 81(24), 34717-34735. https://doi.org/10.1007/s11042-021-11273-5

Dhanabalan, S. P., Abdul Rahaman, S., & Jegankumar, R. (2021). Flood monitoring using Sentinel-1 sar data: A case study based on an event of 2018 and 2019 Southern part of Kerala. The International Archives of the Photogrammetry. *Remote Sensing and Spatial Information Sciences*, 44, 37-41. https://doi.org/10.5194/isprs-archives-XLIV-M-3-2021-37-2021

Fakhri, F., & Gkanatsios, I. (2025). Quantitative evaluation of flood extent detection using attention U-Net case studies from Eastern South Wales Australia in March 2021 and July 2022. *Scientific Reports*, 15(1), 12377. https://doi.org/10.1038/s41598-025-92734-x

Gale, E. L., & Saunders, M. A. (2013). The 2011 Thailand flood: climate causes and return periods. *Weather*, 68(9), 233-237. https://doi.org/10.1002/wea.2133

Ghosh, B., Garg, S., Motagh, M., & Martinis, S. (2024). Automatic flood detection from Sentinel-1 data using a nested UNet model and a NASA benchmark dataset. PFG–Journal of Photogrammetry. *Remote Sensing and Geoinformation Science*, 92(1), 1-18. https://doi.org/10.1007/s41064-024-00275-1

Ghozali, A., Ariyaningsih, Sukmara, R. B., & Aulia, B. U. (2016). A comparative study of climate change mitigation and adaptation on flood management between Ayutthaya City (Thailand) and Samarinda City (Indonesia). *Procedia-Social and Behavioral Sciences*, 227, 424-429. https://doi.org/10.1016/j.sbspro.2016.06.096

Haidu I., El Orfi T., Magyari-Sáska Z., Lebaut S., El Gachi M. (2024), Modeling the Long-Term Variability in the Surfaces of Three Lakes in Morocco with Limited Remote Sensing Image Sources. *Remote Sensing*, 16 (17), 3133. https://doi.org/10.3390/rs16173133

Hassan, S. M., & Maji, A. K. (2024). Pest Identification based on fusion of Self-Attention with ResNet. *IEEE Access*, 12, 6036-6050. https://doi.org/10.1109/ACCESS.2024.3351003

He, K., Zhang, X., Ren, S., & Sun, J. (2016). Deep residual learning for image recognition. *Proceedings of the IEEE conference on computer vision and pattern recognition*, pp. 770-778. https://doi.org/10.1109/CVPR.2016.90

Hirabayashi, Y., Mahendran, R., Koirala, S., Konoshima, L., Yamazaki, D., Watanabe, S., Kim, H., & Kanae, S. (2013). Global flood risk under climate change. *Nature climate change*, 3(9), 816-821. https://doi.org/10.1038/nclimate1911

Intarat, K., Nuengjumnong, N., Sae-Jung, J., Jangsawang, W., Yoomee, P., & Panboonyuen, T. (2024). Deep Residual Neural Networks with Self-Attention for Landslide Susceptibility Mapping in Uttaradit Province, Thailand. *2024 Geoinformatics for Spatial-Infrastructure Development in Earth and Allied Sciences (GIS-IDEAS)*, IEEE. pp. 1-6. https://doi.org/10.1109/GIS-IDEAS63212.2024.10990879

Jamali, A., Roy, S. K., Beni, L. H., Pradhan, B., Li, J., & Ghamisi, P. (2024). Residual wave vision U-Net for flood mapping using dual polarization Sentinel-1 SAR imagery. *International Journal of Applied Earth Observation and Geoinformation*, 127, 103662. https://doi.org/10.1016/j.jag.2024.103662

Konapala, G., Kumar, S. V., & Ahmad, S. K. (2021). Exploring Sentinel-1 and Sentinel-2 diversity for flood inundation mapping using deep learning. *ISPRS Journal of Photogrammetry and Remote Sensing*, 180, 163-173. https://doi.org/10.1016/j.isprsjprs.2021.08.016

Konovalenko, I., Maruschak, P., Brezinová, J., Prentkovskis, O., & Brezina, J. (2022). Research of U-Net-based CNN architectures for metal surface defect detection. *Machines*, 10(5), 327. https://doi.org/10.3390/machines10050327

Lee, Y., Sim, W., Park, J., & Lee, J. (2022). Evaluation of hyperparameter combinations of the U-net model for land cover classification. *Forests*, 13(11), 1813. https://doi.org/10.3390/f13111813

Li, W., Xiao, Z., Liu, J., Feng, J., Zhu, D., Liao, J., Yu, W., Qian, B., Chen, X., Fang, Y., & Li, S. (2023). Deep learning-assisted knee osteoarthritis automatic grading on plain radiographs: the value of multiview X-ray images and prior knowledge. *Quantitative Imaging in Medicine and Surgery*, 13(6), 3587. https://doi.org/10.21037/qims-22-1250

Liu, J., Liu, K., & Wang, M. (2023). A residual neural network integrated with a hydrological model for global flood susceptibility mapping based on remote sensing datasets. *Remote Sensing*, 15(9), 2447. https://doi.org/10.3390/rs15092447

Liu, Z., Chen, B., & Zhang, A. (2020). Building segmentation from satellite imagery using U-Net with ResNet encoder. *2020 5th International Conference on Mechanical*, Control and Computer Engineering *(ICMCCE)*, IEEE. pp. 1967-1971. https://doi.org/10.1109/ICMCCE51767.2020.00431

Liu, Z., Coleman, N., Patrascu, F. I., Yin, K., Li, X., & Mostafavi, A. (2025). Artificial intelligence for flood risk management: A comprehensive state-of-the-art review and future directions. *International Journal of Disaster Risk Reduction*, 117, 105110. https://doi.org/10.1016/j.ijdrr.2024.105110

Loc, H. H., Park, E., Chitwatkulsiri, D., Lim, J., Yun, S. H., Maneechot, L., & Phuong, D. M. (2020). Local rainfall or river overflow? Re-evaluating the cause of the Great 2011 Thailand flood. *Journal of Hydrology*, 589, 125368. https://doi.org/10.1016/j.jhydrol.2020.125368

Magyari-Sáska, Z., Haidu, I., & Magyari-Sáska, A. (2025). Experimental Comparative Study on Self-Imputation Methods and Their Quality Assessment for Monthly River Flow Data with Gaps: Case Study to Mures River. *Applied Sciences*, 15(3), 1242. https://doi.org/10.3390/app15031242

Melgar-García, L., Martínez-Álvarez, F., Bui, D. T., & Troncoso, A. (2023). A novel semantic segmentation approach based on U-Net, WU-Net, and U-Net++ deep learning for predicting areas sensitive to pluvial flood at tropical area. *International Journal of Digital Earth*, 16(1), 3661-3679. https://doi.org/10.1080/17538947.2023.2252401

Misra, A., White, K., Nsutezo, S. F., Straka III, W., & Lavista, J. (2025). Mapping global floods with 10 years of satellite radar data. *Nature Communications*, 16(1), 5762. https://doi.org/10.1038/s41467-025-60973-1

Mosinska, A., Marquez-Neila, P., Koziński, M., & Fua, P. (2018). Beyond the pixel-wise loss for topology-aware delineation. *Proceedings of the IEEE conference on computer vision and pattern recognition*. pp. 3136-3145. https://doi.org/10.1109/CVPR.2018.00331

Mukherjee, A., Nandurbarkar, D., Yadav, H., & Vasa, J. (2024, August). Improvement in Image Segmentation for Flood Images Using UNet and U2Net. *International Conference on ICT for Sustainable Development*, Singapore: Springer Nature Singapore. pp. 321-331. https://doi.org/10.1007/978-981-97-8526-1_25

Munpa, P., Kittipongvises, S., Phetrak, A., Sirichokchatchawan, W., Taneepanichskul, N., Lohwacharin, J., & Polprasert, C. (2022). Climatic and hydrological factors affecting the assessment of flood hazards and resilience using modified UNDRR indicators: Ayutthaya, Thailand. *Water*, 14(10), 1603. https://doi.org/10.3390/w14101603

Muszynski, M., Hölzer, T., Weiss, J., Fraccaro, P., Zortea, M., & Brunschwiler, T. (2022). Flood event detection from sentinel 1 and sentinel 2 data: Does land use matter for performance of U-net based flood segmenters?. *2022 IEEE International Conference on Big Data (Big Data)*, IEEE. pp. 4860-4867. https://doi.org/10.1109/BigData55660.2022.10020911

Pan, Y. (2023). Effect of the deep residual networks at different depths on expression recognition. *Proceedings of the 5th International Conference on Computing and Data Science.* pp. 128-133. https://doi.org/10.54254/2755-2721/21/20231131

Pech-May, F., Aquino-Santos, R., & Delgadillo-Partida, J. (2023). Sentinel-1 SAR images and deep learning for water body mapping. *Remote Sensing*, 15(12), 3009. https://doi.org/10.3390/rs15123009

Pech-May, F., Aquino-Santos, R., Álvarez-Cárdenas, O., Lozoya Arandia, J., & Rios-Toledo, G. (2024). Segmentation and visualization of flooded areas through sentinel-1 images and u-net. *IEEE Journal of Selected Topics in Applied Earth Observations and Remote Sensing*, 17, 8996-9008. https://doi.org/10.1109/JSTARS.2024.3387452

Ponmani, E., & Saravanan, P. (2021). RETRACTED ARTICLE: Image denoising and despeckling methods for SAR images to improve image enhancement performance: a survey. *Multimedia Tools and Applications*, 80(17), 26547-26569. https://doi.org/10.1007/s11042-021-10871-7

Ronneberger, O., Fischer, P., & Brox, T. (2015). U-net: Convolutional networks for biomedical image segmentation. *International Conference on Medical image computing and computer-assisted intervention*, Springer international publishing. pp. 234-241. https://doi.org/10.1007/978-3-319-24574-4_28

Safarov, F., Temurbek, K., Jamoljon, D., Temur, O., Chedjou, J. C., Abdusalomov, A. B., & Cho, Y.-I. (2022). Improved agricultural field segmentation in satellite imagery using TL-ResUNet architecture. *Sensors*, 22(24), 9784. https://doi.org/10.3390/s22249784

Sazara, C., Cetin, M., & Iftekharuddin, K. M. (2019). Detecting floodwater on roadways from image data with handcrafted features and deep transfer learning. *2019 IEEE Intelligent Transportation Systems Conference (ITSC)*, IEEE. pp. 804-809. https://doi.org/10.1109/ITSC.2019.8917368

Shokati, H., Seufferheld, K. D., Fiener, P., & Scholten, T. (2025). Rapid Flood Mapping from Aerial Imagery Using Fine-Tuned SAM and ResNet-Backboned U-Net. *EGUsphere*, 1-20. https://doi.org/10.5194/egusphere-2025-3146

Shoko, C., & Dube, T. (2024). A review of remote sensing of flood monitoring and assessment in southern Africa. *Physics and Chemistry of the Earth*, *Parts A/B/C*, 136, 103796. https://doi.org/10.1016/j.pce.2024.103796

Sibandze, P., Kalumba, A. M., Aljaddani, A. H., Zhou, L., & Afuye, G. A. (2025). Geospatial Mapping and Meteorological Flood Risk Assessment: A Global Research Trend Analysis. *Environmental Management*, 75, 137–154. https://doi.org/10.1007/s00267-024-02059-0

Torti, J. (2012). Floods in Southeast Asia: A health priority. *Journal of global health*, 2(2), 020304. https://doi.org/10.7189/jogh.02.020304

Wang, F., & Feng, X. (2025). Flood change detection model based on an improved U-net network and multi-head attention mechanism. *Scientific Reports*, 15(1), 3295. https://doi.org/10.1038/s41598-025-87851-6

Wang, L., Cui, S., Li, Y., Huang, H., Manandhar, B., Nitivattananone, V., Fang, X., & Huang, W. (2022). A review of the flood management: from flood control to flood resilience. *Heliyon*, 8(11). https://doi.org/10.1016/j.heliyon.2022.e11763

Wu, H., Song, H., Huang, J., Zhong, H., Zhan, R., Teng, X., Qiu, Z., He, M., & Cao, J. (2022). Flood detection in dual-polarization SAR images based on multi-scale deeplab model. *Remote Sensing*, 14(20), 5181. https://doi.org/10.3390/rs14205181

Wu, X., Zhang, Z., Xiong, S., Zhang, W., Tang, J., Li, Z., An, B., & Li, R. (2023). A near-real-time flood detection method based on deep learning and SAR images. *Remote Sensing*, 15(8), 2046. https://doi.org/10.3390/rs15082046

Yadav, R., Nascetti, A., & Ban, Y. (2022). Attentive dual stream siamese u-net for flood detection on multi-temporal sentinel-1 data. *IGARSS 2022-2022 IEEE International Geoscience and Remote Sensing Symposium*, IEEE. pp. 5222-5225. https://doi.org/10.1109/IGARSS46834.2022.9883132

Yang, D., Martinez, C., Visuña, L., Khandhar, H., Bhatt, C., & Carretero, J. (2021). Detection and analysis of COVID-19 in medical images using deep learning techniques. *Scientific Reports*, 11(1), 19638. https://doi.org/10.1038/s41598-021-99015-3

Yang, L., Zhong, J., Zhang, Y., Bai, S., Li, G., Yang, Y., & Zhang, J. (2022). An improving faster-RCNN with multi-attention ResNet for small target detection in intelligent autonomous transport with 6G. *IEEE Transactions on Intelligent Transportation Systems*, 24(7), 7717-7725. https://doi.org/10.1109/TITS.2022.3193909

Zhang, M., Chen, F., Liang, D., Tian, B., & Yang, A. (2020). Use of Sentinel-1 GRD SAR images to delineate flood extent in Pakistan. *Sustainability*, 12(14), 5784. https://doi.org/10.3390/su12145784

Zhao, J., Li, Y., Matgen, P., Pelich, R., Hostache, R., Wagner, W., & Chini, M. (2022). Urban-aware u-net for large-scale urban flood mapping using multitemporal sentinel-1 intensity and interferometric coherence. *IEEE Transactions on Geoscience and Remote Sensing*, 60, 1-21. https://doi.org/10.1109/TGRS.2022.3199036

Zhong, Z., Li, J., Ma, L., Jiang, H., & Zhao, H. (2017). Deep residual networks for hyperspectral image classification. *2017 IEEE international geoscience and remote sensing symposium (IGARSS)*, IEEE. pp. 1824-1827. https://doi.org/10.1109/IGARSS.2017.8127330

Zhou, Z., Rahman Siddiquee, M. M., Tajbakhsh, N., & Liang, J. (2018). Unet++: A nested u-net architecture for medical image segmentation. *International workshop on deep learning in medical image analysis*, Springer International Publishing. pp. 3-11. https://doi.org/10.1007/978-3-030-00889-5_1